PHYSICAL REVIEW B
CONDENSED MATTER

THIRD SERIES, VOLUME 41, NUMBER 10 PART A 1 APRIL 1990

Energy-level assignments for the ^1E and ^3T_1a states of $MgO:Ni^{2+}$

Stephen A. Payne
Lawrence Livermore National Laboratory, University of California, P.O. Box 5508, Livermore, California 94550
(Received 20 November 1989)

The $^1T_2 \rightarrow {}^1E, {}^3T_1a$ luminescence, and the $^3T_2 \rightarrow {}^1E, {}^3T_1a$ excited-state absorption spectra of $MgO:Ni^{2+}$ have been observed for the first time. These data are used in conjunction with the conventional ground-state absorption spectrum, to determine the energy-level assignments for the ^3T_1a and ^1E states. In particular, three of the four spin-orbit components of the ^3T_1a state are identified. Although the A_1 spin-orbit component is broadened beyond recognition, the T_1 component is directly observed as a magnetic-dipole allowed transition in the $^3T_2 \rightarrow {}^3T_1a$ excited-state absorption spectrum. Lastly, the energies of the T_2 and E spin-orbit levels are inferred from the positions of their vibrational sidebands in the ground-state absorption spectrum.

I. INTRODUCTION

The $MgO:Ni^{2+}$ system has a long history of investigation, in part, because the Ni^{2+} impurity is coordinated by a perfect octahedron of oxygen ions in this crystal, and therefore represents a prototypical system for study and testing of theoretical formalisms. $MgO:Ni^{2+}$ was studied by Low three decades ago,[1] and, in this work, he obtained the absorption spectra and assigned the bands to the energy levels of Ni^{2+}. A more thorough theoretical description of Ni^{2+} was then developed by Liehr and Ballhausen, in which the effects of spin-orbit coupling were included, in addition to the crystal-field and electron-electron interactions.[2] Pappalardo *et al.* remeasured the $MgO:Ni^{2+}$ absorption spectra and discovered that many of the spectral bands exhibited significant structure, and that this was particularly pronounced for the case of the $^3A_2 \rightarrow {}^3T_1a$ transition.[3] They attempted to fit the positions of these sharp features using the theory of Liehr and Ballhausen, although their final analysis was probably incorrect, because the vibrational features serve to confuse the assignments of the spin-orbit-split components of the ^3T_1a state. Ralph and Townsend observed the $^3T_2 \rightarrow {}^3A_2$ emission band and recognized that much of the structure was vibrational in origin,[4,5] although it was Manson,[6] and Sangster and McCombie,[7] who conducted a thorough analysis of the vibrational structure, and concluded that the sidebands were primarily composed of odd-parity t_{1u} phonons. A detailed analysis of magnetic circular dichroism experiments by Bird, *et al.* confirmed that the t_{1u} vibrations dominate the vibrational structure.[8] Interestingly, it turns out that the t_{1u} vibrational fine structure can be interpreted in much greater detail for the related system, $CaO:Ni^{2+}$.[9,10] Much work has also involved absorption and emission studies of the Ni^{2+}-doped fluoride crystals, as well.[11–14]

The nature of the fine structure of the ^1E and ^3T_1a bands of the $MgO:Ni^{2+}$ is the topic of the current paper. However, the absorption spectra are now well documented, and no further interpretation would be possible without the infusion of new information. One way to gain further insight into the nature of the ^1E and ^3T_1a states is to study the transitions to these levels from states of Ni^{2+} other than the $^3A_2$ ground state. In this work, we present the $^3T_2 \rightarrow {}^1E, {}^3T_1a$ excited-state absorption (ESA) spectra, as well as the unrelaxed luminescence originating from the $^1T_2$ level and terminating on the ^1E and ^3T_1a. Both of these types of experiments have previously been conducted, although neither have directly involved the ^1E or ^3T_1a states. Specifically, Moncorgé and Benyattou have investigated the ESA spectra from $^3T_2$ to the $^1T_2$ and ^3T_1b states,[15] and Sibley and co-workers have studied the emission from the $^1T_2$ to the $^3A_2$ and $^3T_2$ states.[16] The characterization of the $^1T_2 \rightarrow {}^1E$ and ^3T_1a ESA have previously been neglected because these transitions occur in the infrared, where photomultiplier tubes are not useful, and because both of these experiments suffer from substantial interference from the "normal" $^3T_2 \rightarrow {}^3A_2$ emission band. Figure 1 summarizes the tran-

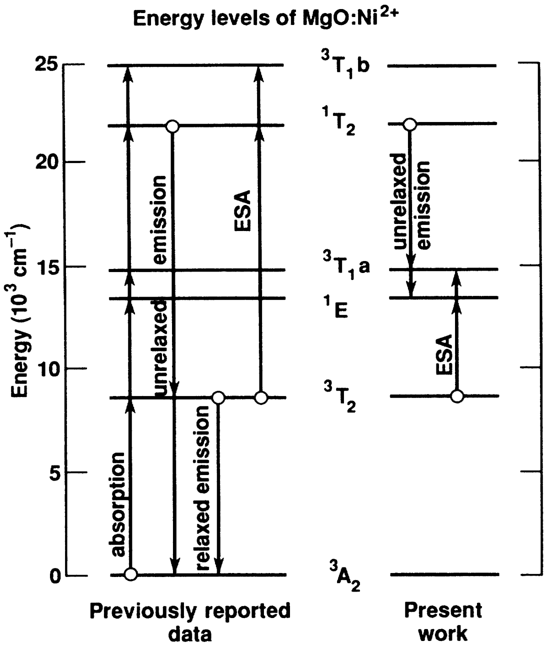

FIG. 1. Description of the ground-state absorption, excited-state absorption (ESA), and relaxed and unrelaxed emission of $MgO:Ni^{2+}$, that have been reported in previous studies, and that appear for the first time in the present work.

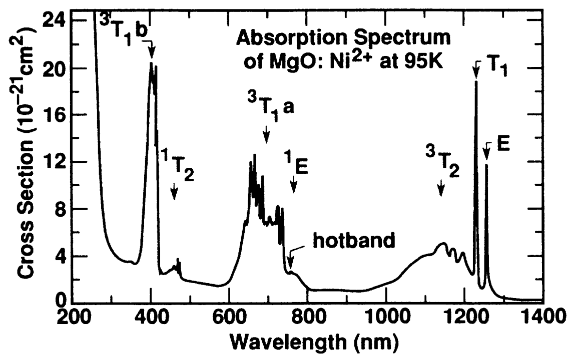

FIG. 2. Absorption spectrum of $MgO:Ni^{2+}$ at 95 K plotted on an absolute cross-section scale. The crystal was 52-mm long and contained 0.25-mol% Ni. The final state for the transitions emanating from the $^3A_2$ ground state are designated on the figure; the E and T_1 spin-orbit components of the $^3T_2$ state are also indicated.

sitions which have previously been investigated, and the transitions which form the focus of the present work.

The $^1T_2 \rightarrow {}^1E$ and $^1T_2 \rightarrow {}^3T_1a$ emissions have been previously observed for the $CsCdCl_3:Ni^{2+}$ crystal.[17] The reported data is surprising, however, since the emission band assigned to the spin-allowed $^1T_2 \rightarrow {}^1E$ transition is observed to be weaker than that assigned to the spin-forbidden $^1T_2 \rightarrow {}^3T_1$ transition. No such reversal of the spin selection rules is observed in the present work. Further investigation is necessary to resolve this issue.

Moulton and others have examined the laser performance of Ni^{2+} in MgF_2 and MgO,[18–21] and have suggested that ESA at the lasing wavelengths is a significant loss mechanism for these lasers. The $^3T_2 \rightarrow {}^3T_1a$ ESA data presented in this paper is the first direct measurement of this ESA band. On the basis of the data in this paper, it appears likely that this ESA will provide a significant loss mechanism for most Ni^{2+} lasers.

II. EXPERIMENTAL RESULTS

A. Ground-state absorption spectra

The absorption spectrum of $MgO:Ni^{2+}$ is displayed in Fig. 2. These data were obtained with a computer-controlled Cary 17 Spectrophotometer. The sample was cooled with a closed-cycle helium refrigeration system for the absorption (and the luminescence) spectra. The spectral features of Fig. 2 are predominantly revolved, as can be determined by comparing the spectrum obtained at 95 K, with data at 14 K. Although a smooth line has been drawn through the data, the noise at wavelengths greater than 770 mm is considerably greater due to a detector change.

The crystal utilized in this work was grown by Dr. Yok Chen at Oak Ridge National Laboratory. The sample had a pathlength of 52 mm and was of good optical quality. The concentration was measured to be 0.25 mol% Ni, which corresponds to 1.35×10^{20} Ni^{2+} ions/cm^3. Using this information, the absorption spectrum of Fig. 2 was set on an absolute cross-section scale.

The identity of the final state of the transitions giving rise to the absorption bands are identified on Fig. 2. These assignments are well known, and correspond to the energy levels of Fig. 1. The E and T_1 spin-orbit components of the $^3T_2$ state are also indicated on Fig. 2. The E and T_1 zero-phonon lines can be observed at 8003 and 8178 cm^{-1} because the $^3A_2 \rightarrow {}^3T_2$ transition is magnetic dipole allowed. Two additional spin-orbit lines are expected for the $^3T_2$ at higher energy, although their exact positions are uncertain due to the overlapping vibronic structure.

The ^3T_1a and ^1E states are seen in Fig. 2 to overlap in the 600–800 nm region. Since the $^3A_2 \rightarrow {}^1E, {}^3T_1a$ transitions are magnetic-dipole forbidden, the zero-phonon line cannot be observed in the ground-state absorption spectrum. Most of the sharp peaks in this region have been shown to be due to the t_{1u} vibrational density of states.[6–8] The small peak at 751 nm has been interpreted to be a t_{1u} vibrational hot band of the $^3A_2 \rightarrow {}^3T_1a$ transition, and therefore suggests that the forbidden origin is located halfway between this feature and the first prominent line of the ^3T_1a state.

The spin-forbidden $^3A_2 \rightarrow {}^1T_2$ transition appears at higher energy, and is rather weak, as expected. The $^1T_2$ state emits in most materials at low temperature.[16] The ^3T_1b is the highest-lying state of Fig. 2.

It is the remarkable structure of the ^3T_1a state that is the focus of the current work. It is due to the presence of phonon sidebands and to the spin-orbit splitting of the ^3T_1a state, while the ^1E level appears as a weaker band at lower energy. In order to gain further insight into the ^3T_1a and ^1E states, we studied the $^1T_2 \rightarrow {}^3T_1a$, ^1E emissions, and the $^3T_2 \rightarrow {}^1E, {}^3T_1a$, excited-state absorption processes. This new information will be used, in conjunction with the $^3A_2 \rightarrow {}^1E, {}^3T_1a$, absorption pictured in Fig. 2, to develop a better understanding of these states. It is expected to be useful to study transitions to the ^1E and ^3T_1a levels from states other than the $^3A_2$, since there are different selection rules operative, and because the relative geometry of the states in the multicoordinate configuration space is likely to be different.

B. Excited state absorption spectra

The excited state absorption (ESA) spectra were obtained using a setup which was previously described.[22] It is based on the use of a 2-Hz Rhodomine-640 flashlamp-pumped dye laser, which generated 300 mJ/pulse, and pumped the Ni^{2+} ions to their $^3T_2$ excited state. The probe beam consisted of a stable, continuous-wave, tungsten-halogen lamp which was collimated and focused to a spot size smaller than the pump beam (~ 1 mm). A cooled InAs detector, operating in the photovoltaic mode, was amplified and used in conjunction with a box-car to measure the probe beam intensity for several milliseconds immediately following the pump pulse, (since the $^3T_2$ lifetime[21] is 3.5 ms). A computer operated a system of shutters in order to determine the small change in probe intensity that resulted from the presence of the pump beam. To do this, the effects of sample emission and electronic noise had to be carefully taken into account. The ESA scan of Fig. 3 had to, nevertheless, be truncated at 1600 nm because the pump-induced $^3T_2 \rightarrow {}^3A_2$ emission began to overwhelm the detection system, such that the probe beam intensity could not be accurately measured. The data in Fig. 3 involved probe beam intensity changes on the order of 0.3%. In order to minimize the random noise level, six separate scans, each requiring 1–2 h of accumulation time, were obtained and then averaged together. The ESA spectra were set to an absolute cross section scale by comparing the bleaching signal of the $^3A_2 \rightarrow {}^3T_2$ transition (of known cross section) with the magnitude of the ESA signal.[22]

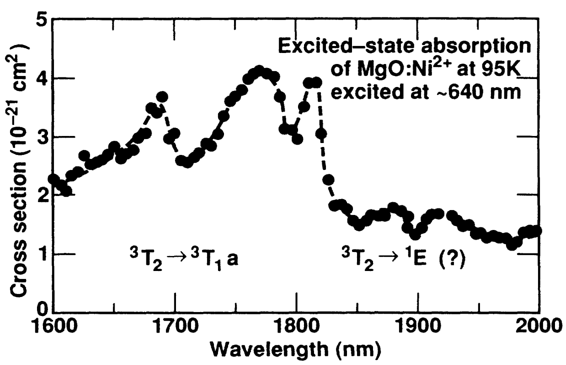

FIG. 3. $^3T_2 \rightarrow {}^3T_1a$, ^1E excited-state absorption spectrum of MgO:Ni^{2+} obtained at 95 K. The sharp feature at 1810 mm is due to the $E(^3T_2) \rightarrow T_1(^3T_1a)$ transition, and the broader features at 1770 and 1690 mm are vibronic sidebands. The baseline offset between 1850–2000 mm may be due, in part, to the $^3T_2 \rightarrow {}^1E$ transition, although it is probably mostly of instrumental origin.

The peaks observed at wavelengths shorter than 1850 nm are clearly due to the transitions from the $^3T_2$ state, to the ^3T_1a. The exact nature of this transition will be pursued further in Sec. III. The offset from the baseline at $\lambda > 1850$ nm may be due, in part, to the $^3T_2 \rightarrow {}^1E$ transition, as this is energetically reasonable on the basis of the energies of the states shown in Figs. 1 and 2. In addition, when we measured the probe intensity changes occurring 10 ms following the pump pulse (after the Ni^{2+} excited state have completely decayed away), the signal was indeed zero. Yet, in a separate experiment, it was found that the spectrum does not approach zero, even at wavelengths as long as 2500 nm, as it should. Therefore, it is assumed at this time that a significant portion of the baseline shift is due to an optical artifact, such as thermal lensing.

C. Unrelaxed luminescence spectra

From energy levels shown in Figs. 1 and 2, we may predict that the $^1T_2 \rightarrow {}^1E, {}^3T_1a$ luminescence will be in the wavelength range of 1–2 μm. As a result, we used a InAs detector and a monochromator grating blazed at 1 μm, to characterize this emission. An LD-390 dye laser was pumped by the tripled output of an yttrium aluminum garnet (YAG) laser and tuned to 389.4 mm to provide the excitation pulse, such that the ^3T_1b state was excited. The energy in the ^3T_1b relaxes rapidly to the $^1T_2$ metastable level, which has a lifetime of 27 μs at low temperature. The short lifetime of the $^1T_2$ is probably mostly due to nonradiative relaxation, which eventually populates the $^3T_2$ excited state. The lifetime of the $^1T_2$ state may also be influenced by the presence of concentration quenching.[17,18] The $^3T_2$ state is metastable and has a lifetime of 3.5 ms at low temperature.[21] The main experimental problem encountered involves the fact that the $^1T_2 \rightarrow {}^1E, {}^3T_1a$ emission, which we intend to observe, is expected to overlap the "normal" $^3T_2 \rightarrow {}^3A_2$ emission.[4–6] This difficulty can be overcome, in principle, by exciting the $^1T_2$ state, and comparing the ensuing emission that occurs on a short time scale (while the $^1T_2$ is still populated), with the emission spectrum that is obtained directly following the decay of the $^1T_2$ state to the $^3T_2$, and then subtracting the two spectra. The pure $^1T_2 \rightarrow {}^1E, {}^3T_1a$ spectrum should be obtainable in this manner.

The results of the procedure described above are shown in Fig. 4. The detector had a time response of about 50 μs and thus was adequate for our purposes. Although the spectra have not been corrected for the spectral response of the monochromator and detector, both have optimum sensitivity in the near infrared, and the overall response is relatively flat in the 1–2-μm region. The short-lived emission spectrum measured following a 80-μs delay is displayed in the middle frame, while the emission observed after 200 μs appears in the lowest frame. This 200-μs delay spectrum arises solely from the

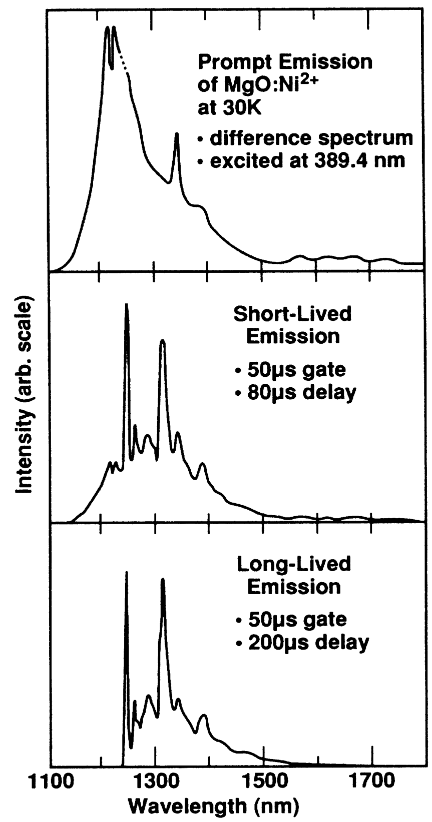

FIG. 4. $^1T_2$ luminescence spectra of $MgO{:}Ni^{2+}$ obtained at 20 K. The spectrum obtained with gated detection set at an 80-μs delay appears in the middle frame, and is due to a mixture of the $^1T_2 \rightarrow {}^1E, {}^3T_1a$ and $^3T_2 \rightarrow {}^3A_2$ emissions. The pure $^3T_2 \rightarrow {}^3A_2$ spectrum is obtained with a 200-μs delay, as shown in the lowest frame. The subtraction of these two spectra separates out the $^1T_2 \rightarrow {}^1E, {}^3T_1a$ spectrum, as seen in the upper frame. The broad band is due to the $^1T_2 \rightarrow {}^1E$ transition, and the prominent sharp features arise from resonance effects occurring between the ^3T_1a and ^1E states. The sharp negative feature is an artifact due to reabsorption of light by the Ni^{2+} ions (see Fig. 2).

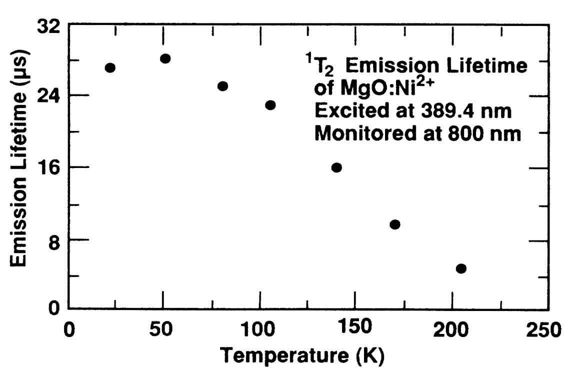

FIG. 5. Lifetime of the $^1T_2$ state as a function of temperature as determined by monitoring the $^1T_2 \rightarrow {}^3T_2$ emission. The emission is probably mostly nonradiative at low temperature, and it is found to quench further as the temperature rises.

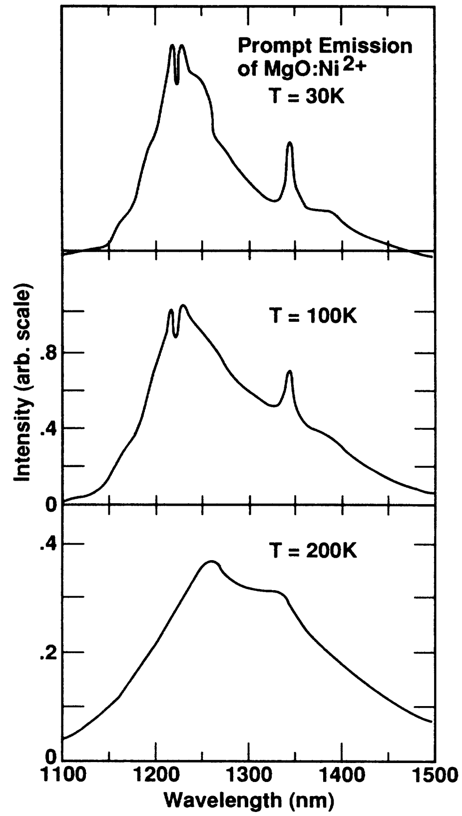

FIG. 6. $^1T_2 \rightarrow {}^1E, {}^3T_1$ emission spectra of $MgO{:}Ni^{2+}$ obtained at the three indicated temperatures, using the subtraction procedure demonstrated in Fig. 4. Notice that the overall intensity decreases, as the temperature rises.

$^3T_2 \rightarrow {}^3A_2$ transition. By matching the intensity of the line at 1250 nm and subtracting the spectra, the result in the upper frame is derived. (The small region of the spectrum that is dashed is drawn to deemphasize a derivative-like artifact that results from a small wavelength miscalibration between the 1250-nm sharp line of the short- and long-lived spectra.) The sharp dip at 1214 nm is an artifact due to reabsorption of light by the Ni^{2+} ions (see Fig. 2). The peaks at 1339 and 1383 mm, and the weak features between 1550 and 1750 mm, were all found to be reproducible. The main broad emission band is due to the $^1T_2 \rightarrow {}^1E$ transition, while the sharp features arise from the $^1T_2$ transitions to the spin-orbit components of the ^3T_1a state. These assignments will be discussed in detail in Sec. III.

In order to confirm the identity of the originating state for the emission band shown in the upper frame of Fig. 4, the temperature dependence of the emission intensity was compared with the emission lifetimes of the well-known $^1T_2 \rightarrow {}^3T_2$ transition.[16] The lifetimes of the $^1T_2$ state were determined with the aid of a photomultiplier tube; these results appear in Fig. 5. The rather short lifetime of 27 μs at 22 K indicates that nonradiative decay and/or cross relaxation are significant at low temperatures, since the radiative lifetime is likely to be of the order of a millisecond. It is also apparent that the luminescence yield decreases further as the temperature rises.

Fig. 6 contains the $^1T_2 \rightarrow {}^1E, {}^3T_1a$ spectra at 30, 100, and 200 K. These data provide two pieces of information. Firstly, it is evident that the emission intensity drops by 2.5 in passing from 100 K to 200 K. This is similar to the decrease of approximately 4 observed for the lifetime in Fig. 5, although it is not identical. (The emission intensity is not exactly quantitatively related at different temperatures because of the slow time response of the detector.) The second observation from Fig. 6 is that the sharp features seen in the upper frame appear to broaden as the temperature is increased.

III. INTERPRETATION OF RESULTS

Section II contains spectral data involving transitions that emanate from the $^3A_2$ (ground-state absorption), $^3T_2$ (excited-state absorption), and $^1T_2$ (unrelaxed luminescence), and terminate on the ^3T_1a and ^1E states. The purpose at this section is to interpret the peaks and bands that were observed, on the basis of the relevant selection rules. In order to pursue this goal, we first plot in Fig. 7 all of the spectra on the same energy scale, which is relative to the $^3A_2$ ground state. This was accomplished by adding the energy of the lowest spin-orbit level of the $^3T_2$ state at 8003 cm^{-1} to the excited state absorption (ESA) spectrum, and similarly subtracting the unrelaxed luminescence spectrum from the energy of $^1T_2$ origin at 21126 cm^{-1}.[23]

Prior to the present work, the main information available concerning the ^1E and ^3T_1a states was the absorption spectrum (shown in the lowest frame of Fig. 7). Additionally, it is known that the structure observed for the ^3T_1a state is predominantly due to the t_{1u} phonons; the $^3A_2 \rightarrow {}^3T_1a$ transition is magnetic-dipole forbidden. The ^3T_1a state is expected to be composed of four spin-orbit levels, including the A_1, T_1, T_2, and E levels, from lower to higher energy. As a result, the most reasonable previous assignment was that each "pair" of lines in Fig. 7 (designated as 4,5; a,b; 6,7; and 8,9 in the figure), was the vibrational sideband for each of the four spin-orbit origins.[8] Furthermore, these energy levels roughly correspond to the results of crystal-field calculations. Perhaps the only troubling aspect of this assignment involves the question as to why the peaks labeled a and b in Fig. 7 are so much weaker than the others. In fact, if we did not "need" to find another spin-orbit level, it would probably be most natural to assign peaks a, b, and c as the continuation of the phonon structure arising from the origin responsible for peaks 4 and 5.

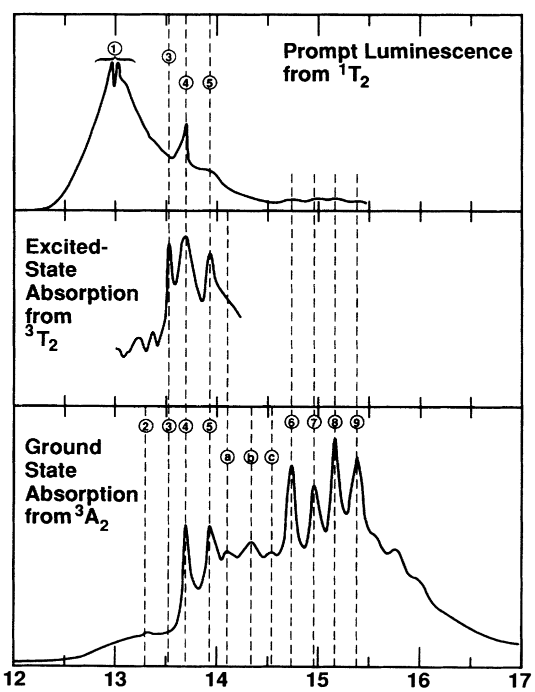

FIG. 7. Summary of the spectra in Figs. 2, 3, and 4 relating to the ^1E and ^3T_1a states, in which the energy levels have all been plotted relative to the energy of the $^3A_2$ ground state. The lines have been assigned as follows: $1={}^1E$ state; $2=t_{1u}$ hot-band of T_1 state; $3=T_1$ origin; 4,5,a,b,c= vibrational sideband of T_1 state; 6,7,= vibrational sideband of T_2 state; 8,9= vibrational sideband of E state.

It is apparent from the data in the middle frame of Fig. 7 that the vibrational peaks labeled 4 and 5 are also observed for the $^3T_2 \rightarrow {}^3T_1a$ ESA transition, although there is an additional feature (No. 3) at slightly lower energy. In what follows, the various possible interpretations of peak 3 are now considered. The first inclination is to suspect that it is an electronic origin, since the $^3T_2 \rightarrow {}^3T_1a$ transition is, in general, magnetic-dipole allowed. However, in considering the selection rules for the spin-orbit components of the particular transition at hand based on the assignments of Bird, *et al.*,[8] we find that the $E(^3T_2) \rightarrow A_1(^3T_1a)$ transition is forbidden, and therefore this origin should not have been observed in our ESA spectrum.

Another possibility is that feature No. 3 is a hot band, since the ESA data was accumulated at 95 K. The hot band might arise from the T_1 spin-orbit level of the $^3T_2$ state (denoted on Fig. 2) and terminate on the vibrational feature labeled 4 in Fig. 7. Although the energy differences match well for this assignment, several inconsistencies remain with this interpretation. First, its relatively narrow width of 50 cm^{-1} (partly instrument limited) suggests that it is not a vibrational sideband. Secondly, the Boltzmann factor predicts that feature 3 should exhibit 7% of the intensity found for No. 4 if it were a hot band; this relative intensity should be mainly evidenced in terms of different peak heights. As a result of the preceding discussion the hot-band assignment seems unlikely.

Our preferred interpretation of the ESA data is at variance with the original assignments of Bird, *et al.*[8] It is suggested here that feature No. 3 arises from the $E(^3T_2) \rightarrow T_1(^3T_1a)$ transition, since this transition is magnetic-dipole allowed. We then, of course, encounter the new puzzle as to where the lowest-lying A_1 spin-orbit component of the ^3T_1a state is located; this issue will be addressed shortly. It is noted that peak No. 2 is a t_{1u} vibrational hot band corresponding to the vibronic designated No. 4, and therefore the origin is expected to lie halfway between 2 and 4, as feature No. 3 does within experimental error. The entries in Table I indicate that the

TABLE I. Energies of the spin-orbit components (T_1, T_2, E) and vibrational side bands (v_a,v_b) of the ^3T_1a state—see Fig. 7(a).

Label (see Fig. 7)	Experimental data (relative to $^3A_2$) (cm^{-1}) Ground-state absorption	Excited-state absorption	Unrelaxed luminescence	Assignment	s.o. level (implied or average)
2	13 308			T_1-v_a	
3	(13 492)	13 513		T_1	13 503
4	13 675	13 653	13 656	T_1+v_a	
5	13 921	13 938	13 893	T_1+v_b	
				T_2	14 545
6	14 729			T_2+v_a	
7	14 945			T_2+v_b	
				E	14 982
8	15 166			$E+v_a$	
9	15 388			$E+v_b$	

[a]Zero-phonon lines of $^3T_2$ and $^1T_2$ states taken as 8003 and 21 126 cm^{-1}, v_a, and v_b as 184 and 400 cm^{-1}.

T_1 spin-orbit component is expected to occur at 13 492 cm^{-1} on the basis of features 2 and 4 in the absorption spectra, while it is found to be at 13 513 cm^{-1} in the ESA spectrum; the agreement is reasonable since the instrumental resolution is about 25 cm^{-1}. This assignment relieves one from having to rationalize why the peaks labeled a and b appear to be so much weaker than the other pairs of lines in the absorption spectrum. Notice that features a, b, and c are similar in appearance to that which occurs at higher energy from feature 9, supporting the notion that they are simply a continuation of the vibrational structure originated at the zero-phonon line, No. 3. It is also worth noting that the $^1T_2 \rightarrow ^3A_2$ emission exhibits a similar vibrational progression as observed for the 2-3-4-5-a-b-c series of Fig. 7 (compare with the upper part of Fig. 1 in Ref. 16).

Having identified the T_1 spin-orbit origin, the 6, 7 and 8, 9 pairs of vibrational features can be used to determine that the next two higher-lying spin-orbit origins, having T_2 and E symmetry, are at 14 545 and 14 982 cm^{-1}, respectively. In Table I, these assignments are listed, along with the identification of the two vibrational features, referred to as v_a and v_b. The v_a frequency is taken to be 184 cm^{-1}, and this value was used to infer the positions of the T_2 and E origins. At this juncture, we have identified the energies of three of the four spin-orbit levels of the ^3T_1a state: the T_1, T_2, and E levels. The missing A_1 origin cannot be directly observed from either the $^3A_2$ ground state or the $^3T_2$ excited state, since both of the transitions to the A_1 level turn out to be magnetic-dipole forbidden.

The luminescence originating from the $^1T_2$ state is reproduced in the upper frame of Fig. 7. The main, broad band labeled No. 1 is clearly due to the spin-allowed $^1T_2 \rightarrow ^1E$ transition. It coincides well with the onset of the absorption band at 12 500 cm^{-1}, although the absorption appears to reach a "plateau" where the emission spectrum clearly falls in intensity near 13 500 cm^{-1}.

The $^1T_2$ luminescence does exhibit some fine structure, including two peaks (4 and 5), and a series of weak features in the region of 14 500 to 15 500 cm^{-1}. The lines in the 14 500–15 500-cm^{-1} region correspond to features 6–9 in the absorption spectrum; the spin forbidden nature of the $^1T_2 \rightarrow ^3T_1a$ transition accounts for their relative weakness. Peaks 4 and 5 are observed in both the ESA and ground-state absorption spectra, and are therefore associated with the vibronic sidebands building on the T_1 origin. The features labeled 4 and 5 seem unusual, since they appear to be superimposed on a rather smooth band. This type of appearance often indicates the presence of Fano antiresonances, which would arise from the mixing of the ^3T_1a and ^1E states. This phenomenon would account for the relative strength of the T_1 vibronics (4 and 5), compared to those of the T_2 and E spin-orbit states (6–9).

In order for the Fano antiresonances to occur, the line associated with the ^3T_1a state must borrow intensity from the $^1T_2 \rightarrow ^1E$ transition, as the result of some type of mixing interaction. Various interactions have previously been found to be important, depending on the impurity and the electronic states involved. For example, the spin-orbit operator mediates the interaction between the ^2E and $^4T_2$ states for V^{2+} and Cr^{3+},[24,25] while the static crystal field effects the $4f$-$5d$ interaction for Sm^{2+}.[26] In regard to the features labeled 4 and 5 in Fig. 7 no such simple, first-order interaction can be identified. It is therefore inferred that a higher-order process must provide the necessary mixing effect required to observe the Fano antiresonances. The nature of this interaction is not apparent, although it clearly involves higher-order perturbation loops.

The A_1 origin has not been identified among the lines present in the spectra. Since the T_1 origin has been assigned as feature No. 3, it is assumed that the A_1 origin is resonant with the ^1E electronic state. As a result, the A_1 spin-orbit component rapidly relaxes to the ^1E state, thereby broadening the A_1 origin beyond recognition. The overlapping of the $^3A_2 \rightarrow A_1(^3T_1a)$ and $^3A_2 \rightarrow ^1E$ transitions may give rise to the pleateaulike appearance of the absorption spectrum between 12 500 and 13 500 cm^{-1}.

TABLE II. Spin-orbit energy intervals observed for several Ni^{2+}-host systems. The question mark denotes that the energy level separation is not known.

Spin-orbit levels	Energy separation (cm^{-1}) MgO:Ni^{2+} (present work)	CaO:Ni^{2+} [Manson and Wong (Ref. 10)]	$KMgF_3$:Ni^{2+} [Ferguson *et al.* (Ref. 12)]	MgO:Ni^{2+} [Bird, *et al.* (Ref. 8)]
T_1-A_1	?	460	490	400
T_2-T_1	1042	880	849	630
$E-T_2$	437	0	?	450

IV. IMPACT OF $^3T_2 \rightarrow {}^3T_1a$ EXCITED STATE ABSORPTION ON LASER PERFORMANCE

Moulton has examined the laser performance of the Ni^{2+} impurity in MgF_2 and MgO, and has found that the laser efficiency tends to be somewhat lower than expected.[20] He has suggested that ESA at the lasing wavelength may be responsible for the low efficiency; the data in this article supports this contention. A simple calculation using the room temperature emission lifetime and spectrum of MgO:Ni^{2+} gives a peak-emission cross section of 2.0×10^{-21} cm^2. Since the emission band peaks at 1300 nm, we can predict that the vibrational sideband of the $E(^3T_2)\rightarrow E(^3T_1a)$ ESA transition will be falling off into this region. The ESA cross section can be estimated to be about 10^{-21} cm^2 from the data in Fig. 2. Therefore ESA may provide a nonnegligible level of loss at room temperature. The laser may operate more efficiently at lower temperatures, since the emission band exhibits sharp peaks where the emission cross section may become much larger than that of the ESA at the wavelengths of these peaks. The ESA loss level will generally rise as the laser is tuned to larger wavelengths. This situation is similar to the ESA losses found for the d^3 ions, Cr^{3+} and V^{2+}.[22,27]

V. DISCUSSION AND CONCLUSIONS

Table II contains a comparison of the spin-orbit intervals observed for Ni^{2+} in MgO, CaO,[10] and $KMgF_3$;[12] all of these hosts possess sixfold coordinated, cubic substitutional site symmetries. In addition, the previous assignments of MgO:Ni^{2+} by Bird, *et al.*[8] are included, (which involves the assignment of the 4,5; a,b; 6,7; and 8,9 pairs of lines in Fig. 7 as the t_{1u} vibronic sidebands of the A_1, T_1, T_2, and E spin-orbit components, respectively. It should be noted that the E component is very sensitive to the magnitude of the crystal field, and therefore cannot be included in the comparison between the different crystals. The CaO:Ni^{2+} crystal is unique, in that the spin-orbit components can be identified in an unambiguous manner for this system. The interval is on the order of 20–30% larger in MgO, compared to CaO. This increase is larger than one would have anticipated on the basis of reduced covalency in MgO. On the other hand, the previous assignments of Bird, *et al.*[8] place the intervals of MgO as being significantly less than those of CaO and $KMgF_3$. It does not seem possible to base a definitive assignment of the spin-orbit levels solely on the magnitude of the energy intervals, since the previous assignments of Bird, *et al.*[8] and the present assignments appear equally reasonable.

To conclude, our new assignments of the ^1E and ^3T_1a bands are based on the reconciliation of the $^1T_2$ emission data, the $^3T_2$ excited-state absorption spectrum, and the $^3A_2$ ground-state absorption spectrum. Although the assignments of the T_2 and E spin-orbit levels remain unchanged, the A_1 and T_1 levels have been reassigned on the basis of the new ESA and emission data reported in this work and the consideration of the relevant selection rules. The A_1 origin is assumed to be broadened beyond recognition, while the T_1 origin is directly observed as a magnetic-dipole allowed transition in the ESA spectrum. Table I and Fig. 7 summarize these results. The spin-orbit assignments for the ^3T_1a state remain somewhat uncertain at this time, although an alternative assignment scheme has been suggested in this article.

ACKNOWLEDGMENTS

I wish to thank Dr. Yok Chen for growing the MgO:Ni^{2+} crystal, Dr. William Sibley, Professor Donald S. McClure, and Ms. Cecilia Campochiaro for useful discussions and encouragement, Gary Wilke for accumulating all of the data reported in this article, Theresa Duewer for measuring the Ni concentration in the crystal, and Larry Smith for his technical assistance. This research was performed under the auspices of the Division of Materials Sciences of the Office of Basic Energy Sciences, U.S. Department of Energy, and the Lawrence Livermore National Laboratory under Contract No. W-7405-ENG-48. In the course of this work it came to the attention of the author that Stuart Jacobsen of the University of Georgia was also investigating the $^1T_2$ luminescence of MgO:Ni^{2+}. Upon exchanging data we found that our spectra agreed very closely. The author warmly thanks Dr. Jacobsen for his spirit of cooperation and scientific interest.

[1]W. Low, Phys. Rev. **109**, 247 (1958).

[2]A. D. Liehr and C. J. Ballhausen, Ann. Phys. (Paris) **6**, 134 (1959).

[3]R. Pappalardo, D. L. Wood, and R. C. Linares, Jr., J. Chem. Phys. **35**, 1460 (1961).

[4]J. E. Ralph and M. G. Townsend, J. Chem. Phys. **48**, 149 (1968).

[5]J. E. Ralph and M. G. Townsend, J. Phys. C **3**, 8 (1970).

[6]N. B. Manson, Phys. Rev. B **4**, 2645 (1971); N. B. Manson, *ibid.* **4**, 2656 (1971).

[7]M. J. L. Sangster and C. W. McCombe, J. Phys. C **3**, 1498 (1970).

[8]B. D. Bird, G. A. Osborne, and P. J. Stephens, Phys. Rev. B **5**, 1800 (1972).

[9]M. Ishigame and T. Sakurai, J. Phys. Soc. Jpn. **25**, 1629 (1968).

[10]N. B. Manson and K. Y. Wong, J. Phys. C **9**, 611 (1976).

[11]J. Ferguson, H. J. Guggenheim, L. F. Johnson, and H. Kamimura, J. Chem. Phys. **38**, 2579 (1963).

[12]J. Ferguson, H. J. Guggenheim, and D. L. Wood, J. Chem. Phys. **40**, 822 (1964).

[13]J. Ferguson, H. J. Guggenheim, H. Kamimura, and Y. Tanabe; J. Chem. Phys. **42**, 775 (1965).

[14]M. D. Sturge, Solid State Commun. **9**, 899 (1971).

[15]R. Moncorgé and T. Benyattou, Phys. Rev. B **37**, 9186 (1988).

[16]W. E. Vehse, K. H. Lee, S. I. Yun, and W. A. Sibley, J. Luminesc. **10**, 149 (1975); M. V. Iverson and W. A. Sibley, *ibid.* **20**, 311 (1979).

[17]M. Herren, S. Jacobsen, S. May, and H. Güdel, in *Excited States of Transition Elements* (World Scientific, Singapore, 1989), p. 183.

[18]R. Moncorgé, F. Auzel, and J. M. Breteau, Philos. Mag. B **51**, 489 (1985).

[19]L. F. Johnson, H. J. Guggenheim, and R. A. Thomas, Phys. Rev. **149**, 179 (1966).

[20]P. F. Moulton, A. Mooradian, and T. B. Reed, Opt. Lett. **3**, 164 (1978); P. F. Moulton, in *Laser Handbook,* edited by M. Bass and M. L. Stitch, (North-Holland, Amsterdam, 1985), Vol. 5, p. 203.

[21]M. V. Iverson, J. C. Windscheif, and W. A. Sibley, Appl. Phys. Lett. **36**, 183 (1980).

[22]S. A. Payne, L. L. Chase, and G. D. Wilke, Phys. Rev. B **37**, 998 (1988); S. A. Payne, L. L. Chase, W. F. Krupke, and L. A. Boatner, J. Chem. Phys. **88**, 6751 (1988); H. W. H. Lee, S. A. Payne, and L. L. Chase, Phys. Rev. B **39**, 8907 (1989).

[23]The value of 21 126 cm^{-1} for the origin of the $^1T_2$ state can be obtained by subtracting 189 cm^{-1} from the first vibronic observed in the absorption spectrum. The value is corroborated by recent two photon spectra by C. Campochiaro and D. S. McClure in which it was directly observed at 21 134 cm^{-1}, although it appears to be displaced by about 75 cm^{-1} from $^1T_2$ origin reported in Ref. 16.

[24]M. D. Sturge, H. J. Guggenheim, and M. H. L. Pryce, Phys. Rev. B **2**, 2459 (1970).

[25]G. Huber, S. A. Payne, L. L. Chase, and W. F. Krupke, J. Lumin. **39**, 259 (1988).

[26]L. L. Chase, S. A. Payne, and G. D. Wilke, J. Phys. C **20**, 953 (1987).

[27]J. A. Caird, S. A. Payne, P. R. Staver, A. J. Ramponi, L. L. Chase, and W. F. Krupke, IEEE J. Quantum Electron. **QE-24**, 1077 (1988).